

Formation of Amorphous Iron Thin Films during Electrodeposition

M. Saitou

Department of Mechanical Systems Engineering, University of the Ryukyus, 1 Senbaru Nishihara-cho Okinawa, 903-0213, Japan

E-mail: saitou@tec.u-ryukyu.ac.jp

Received: 3 October 2019 / *Accepted:* 6 November 2019 / *Published:* 30 November 2019

In this study, the crystallographic structure transition of iron thin films during electrodeposition (using a rectangular pulse current at a rate of 2 MHz) was investigated using X-ray diffraction (XRD). The mean grain size estimated by the Scherrer equation reached a minimum value for a specific amplitude and duty cycle of the rectangular pulse current; moreover, the minimum grain size decreased with the deposition temperature. The present XRD analysis demonstrated the deposition of amorphous iron films at temperatures ≤ 295 K and duty cycles $\geq 40\%$.

Keywords: Amorphous iron thin film, Rectangular pulse current, Mean grain size, Scherrer equation

1. INTRODUCTION

Amorphous iron materials have attracted great attention owing to their wide applications such as soft magnetism [1], dynamic therapy [2], adsorption and desorption of ions and nutrients [3–4], catalysis [5], and anti-corrosion [6–7]. These materials possess superior properties related to crystallographic isotropy and the absence of grain boundaries.

Electrodeposition is advantageous for the formation of iron thin films because of its low cost and easy production; however, very few studies have focused on the production of amorphous iron electrodeposits [8–9]. Iron thin films are usually composed of α -iron crystalline grains; through electrodeposition, some researchers obtained nano iron-based materials (grain size 25 nm [10]) and nano iron thin films (grain size 27 nm [11]).

The nucleation and growth occurring during electrodeposition have been previously studied [12–14]; in particular, the nucleation occurring at nucleation sites has been assumed to obey the Avrami theorem [15–16] that describes random and homogeneous nucleation. At the thermal equilibrium, the mean distance between kinks has been estimated to be $\sim 4 a_0$ where a_0 is the lattice constant [17]. If the

kinks act as nucleation sites during iron electrodeposition, the mean iron grain size will be ~ 1 nm. A further nucleation mechanism has been proposed [13], which explains the creation of clusters as the result of collision between atoms moving on the material's surface; once stabilized, these clusters would lead to the formation of nuclei.

The number of nucleation sites and clusters affects the grain size; meanwhile, based on the two mechanisms described above, the nuclei should grow through the incorporation of atoms originally moving on the material's surface, leading to an increase of the mean grain size.

The iron thin films electrodeposited using a rectangular pulse current (frequency range from 0.1 to 1 MHz) had a minimum grain size of 13 nm [18]. The grain size of these iron thin films did not increase with the film thickness, indicating an extremely slow grain growth. Hence, when the grain growth is suppressed under specific conditions, the iron electrodeposits will become amorphous. This is our motivation for this study.

The purpose of this study demonstrates the amorphous structures of iron thin films electrodeposited at a rate of 2 MHz.

2. EXPERIMENTAL SET UP

A copper plate of 15×10 mm² and carbon plate of 35×40 mm² were prepared for cathode and anode. A solution containing 1.25 mol/L ferrous sulfate heptahydrate ($\text{Fe}_2\text{SO}_4 \cdot 7\text{H}_2\text{O}$) and 0.86 mol/L potassium sodium tartrate tetrahydrate ($\text{C}_4\text{H}_4\text{KNaO}_6 \cdot 4\text{H}_2\text{O}$) was employed in electrodeposition at a temperature of 276 – 323 K. The solution was strained through a membrane (pore size 0.1 μm) before electrodeposition.

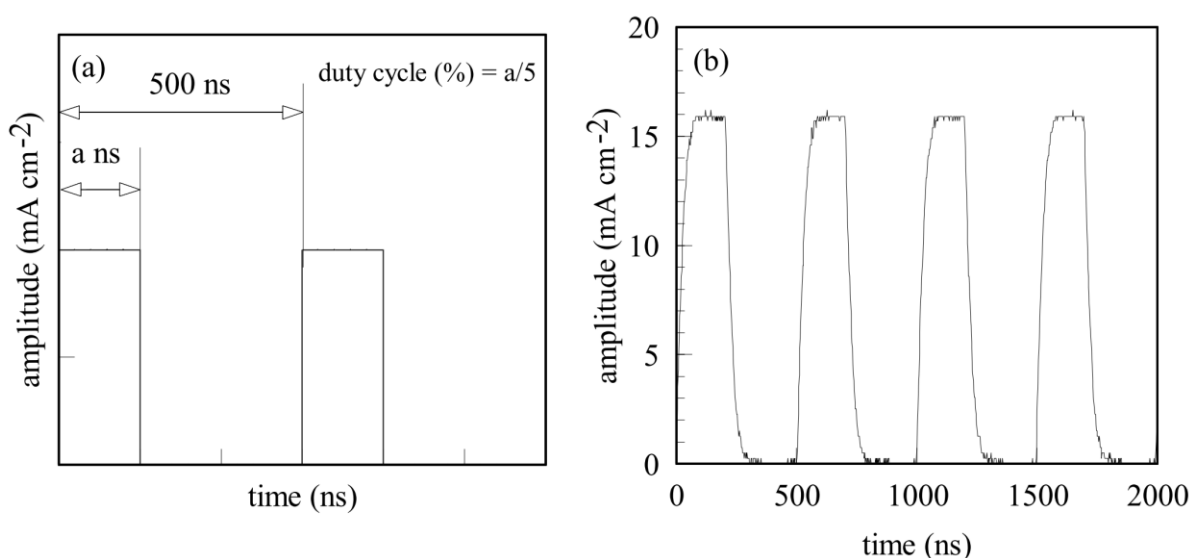


Figure 1. 2MHz rectangular pulse current; (a) schematic plot and (b) observed rectangular pulse current at a duty cycle of 40%.

Figure 1 (a) shows a schematic plot of the 2-MHz rectangular pulse current. A 22- Ω metal film resistor was connected in series with a cell comprising the cathode, anode, and solution. To calculate the rectangular pulse current flowing between the two electrodes, a voltage drop at the metal film resistor was measured with a digital oscilloscope. Figure 1 (b) shows the measured rectangular pulse current (amplitude = 15.9 mAcm⁻², duty cycle = 40 %). The amplitude ranged between 7.8 – 40 mAcm⁻² for the electrodeposition process.

After electrodeposition, the iron thin film produced on the copper plate was rinsed with distilled water and put into a vacuum chamber to avoid oxidization. The iron thin film was observed using scanning electron microscopy (SEM: Hitachi TM3030). The conventional X-ray diffraction (XRD: Rigaku Ultima) with CuK α radiation and a standard θ – 2θ diffractometer with a monochromator of carbon was used to determine the crystallographic structure of the iron thin film on the copper plate.

3. EXPERIMENTAL RESULTS AND DISCUSSION

3.1. Dependence of the mean grain size on the amplitude

Figure 2 shows the XRD charts obtained from the analysis of the 2.8- μ m iron thin films electrodeposited at a duty cycle of 40 % and a temperature of 295 K. Figure 2 (a) shows two diffraction peaks from the (110) and (211) planes of the iron thin films electrodeposited at an amplitude of 7.8 mAcm⁻². This plot indicates that the iron thin film was composed of α -iron crystalline grains with the (110) and (211) planes parallel to the copper plate [19]. At the thermal equilibrium, the surface energy of (110) planes tend to be smaller than that of (211) planes [20]. In this study the growth conditions were far from the thermal equilibrium and the surface energy minimum [21] is not always true.

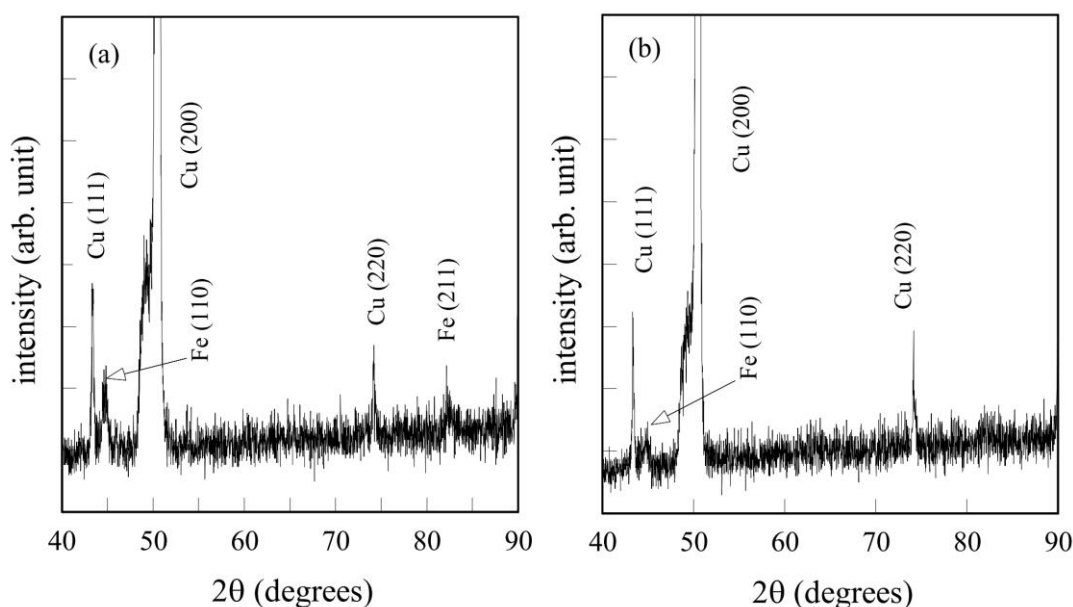


Figure 2. XRD charts obtained from the analysis of the 2.8- μ m iron films electrodeposited at a duty cycle of 40 % and temperature of 295 K (amplitudes = (a) 7.8 mAcm⁻² and (b) 15.9 mAcm⁻²).

Figure 2 (b) shows one diffraction peak from the (110) plane of the iron film electrodeposited at an amplitude of 15.9 mAcm^{-2} . The diffraction peak strength from the (110) plane in Fig 2 (b) is smaller than that in Fig. 2 (a). The iron film was composed of crystalline grains with only the (110) plane parallel to the copper plate.

The Scherrer equation [22] was used to estimate the mean grain size of the iron thin films. Figure 3 shows the dependence of their mean grain size on the amplitude. The iron thin films were electrodeposited at a duty cycle of 40%, (i.e., during one cycle of 500 ns, the current flowed for only 200 ns) and the mean grain size reached a minimum value at 15.9 mAcm^{-2} .

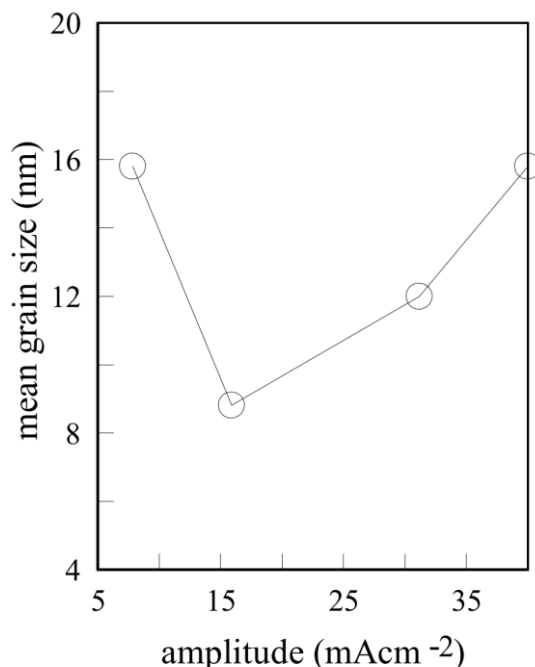


Figure 3. Dependence of the mean grain size of the iron thin films on the amplitude. These iron thin films were electrodeposited at a temperature of 295 K and a duty cycle of 40%.

The nucleation occurs at nucleation sites [13]. For example, kinks in the steps on the surface are considered to be the nucleation site [17]. At the thermal equilibrium, as stated in the Introduction, the mean distance between kinks is estimated to be $4 a_0$. Therefore, if the mean grain size is less than 1 nm, the density of the nucleation site will be more than 10^{14} cm^{-2} . The density of some iron nucleation sites reported in a previous study [23] was of $\sim 10^{11} \text{ cm}^{-2}$, which suggests a mean grain size of 30 nm. In addition, none of the nucleation sites acted as active sites and some of them could not capture any of the moving iron atoms.

The iron atoms moving on the surface can easily collide into each other, forming clusters that do not need nucleation sites in order to become nuclei. An increase in the number of iron clusters or of the nuclei nucleated at the nucleation sites leads to a grain size decrease. At the same time, the nuclei tend to attract and capture moving iron atoms, leading to a grain size increase [24].

Hence, the two-opposite effects on the grain size yield a minimum value of the mean grain size. The decrease in the mean grain size shown in Fig. 3 could have been caused by the formation of nuclei

formation at the nucleation sites and the occurrence of collisions, while the following increase could have been caused by the growth of nuclei.

3.2. Effect of the deposition temperature and duty cycle on the mean grain size

Figures 4 (a) and (b) show the XRD charts obtained for the iron thin films electrodeposited at duty cycles of 20 % and 60 %, respectively. The films were electrodeposited at a temperature of 295 K and an amplitude of 15.9 mAcm^{-2} . Figure 4 (a) shows only a diffraction peak from the (110) plane [18]. All the iron grains with the (110) plane parallel to the copper plate grew in the $\langle 110 \rangle$ direction. Figure 4 (b) shows no diffraction peak from the iron crystallographic planes. This demonstrates that the decrease in the grain size was not counteracted by an increase in the grain growth, leading to an amorphous structure. The copper atoms of the copper electrode can slightly affect the location of the iron atoms electrodeposited on the copper electrode itself. This effect, however, is usually limited within several atomic layers: the crystallographic structure of the copper cathodes should have not affected that of the iron thin films during this experiment.

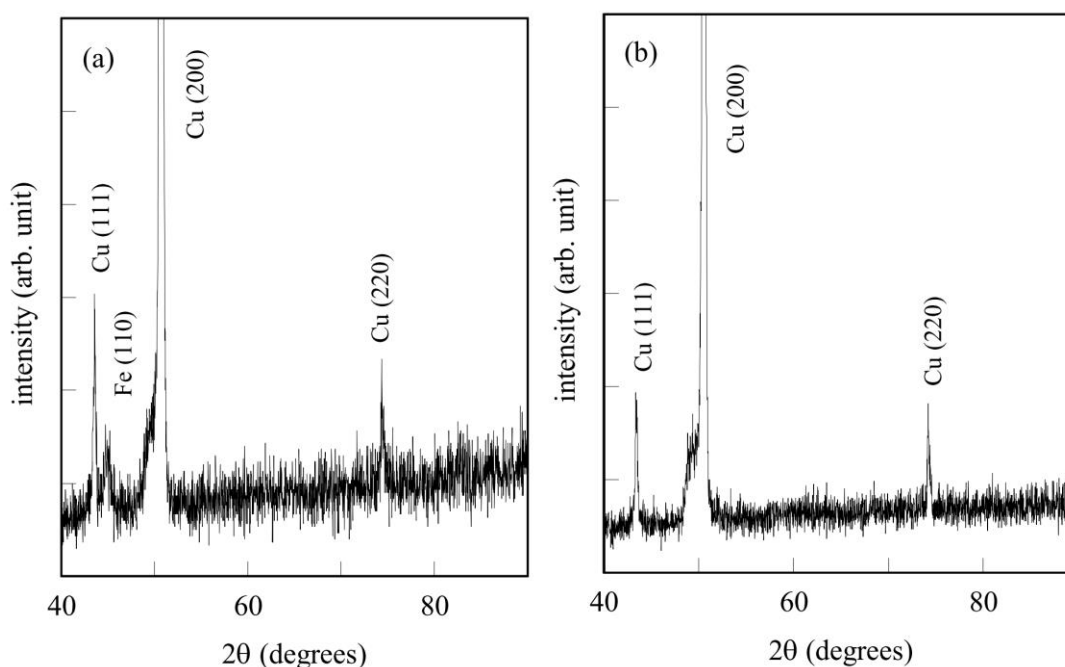


Figure 4. XRD charts obtained for the 2.8- μm iron thin films electrodeposited at an amplitude of 15.9 mAcm^{-2} and duty cycles of (a) 20 % and (b) 60 %.

Figure 5 shows the dependence of the mean grain size on the duty cycle under three deposition temperatures of 276, 295, and 313 K. The iron thin films were electrodeposited at an amplitude of 15.9 mAcm^{-2} . The duty cycle affected the grain size in the same way as the amplitude in Fig. 3; the mean grain size reached its minimum value under the deposition temperatures of 295 and 313 K. It is noted that the mean grain size of zero plotted at the deposition temperatures of 276 and 295 K means no

diffraction peak in the XRD chart of the iron thin films as shown in Fig. 4 (b). The XRD charts of the iron thin films electrodeposited at a deposition temperature of 276 K showed no diffraction peak at a duty cycle more than 40 %. This demonstrates that the iron films electrodeposited under these experimental conditions have amorphous structures.

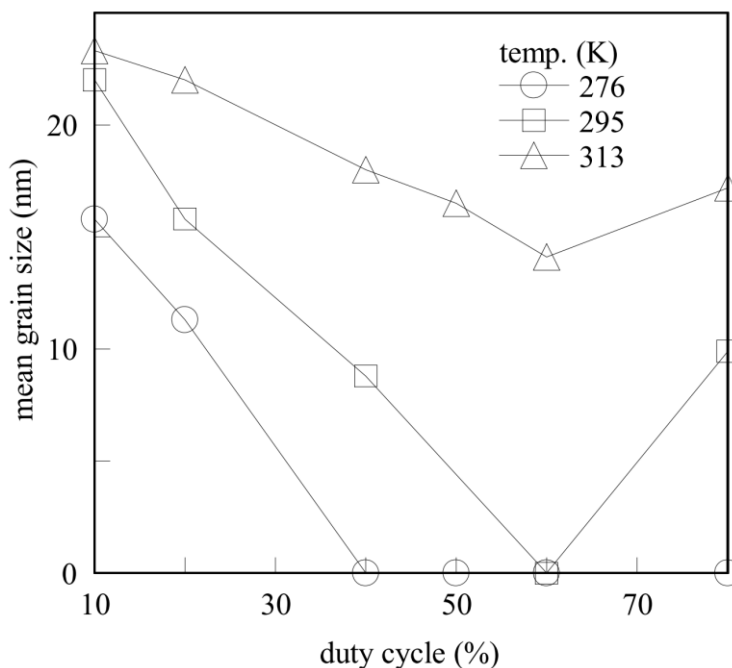


Figure 5. Dependence of the mean grain size of the iron thin films on the duty cycle. The films were electrodeposited at an amplitude of 15.9 mAcm^{-2} and deposition temperatures of 276, 295, and 313 K.

Figure 5 also shows that a decrease in the deposition temperature causes a decrease of the mean grain size. According to the law of energy equipartition [25], the kinetic energy of a particle with one degree of freedom is equal to $k_B T/2$ where k_B is the Boltzmann's constant and T is the absolute temperature. Hence, an iron atom moving on a surface at a temperature of 276 K should have a lower kinetic energy than at 313 K. In fact, a moving iron atom with a large kinetic energy is less likely to be captured within a nucleation site than one with a low kinetic energy: an iron atom with a larger kinetic energy has also a higher probability of overcoming the potential created by the nucleation site. Owing to an increase in the number of nuclei produced by iron atoms with relatively lower kinetic energies, the mean grain size tends to decrease under low temperatures. In addition, the collision between iron atoms with relatively low kinetic energy increases the number of iron clusters. For these reasons, a lower deposition temperature results in a decrease of the mean grain size. The presence of the sufficient number of nucleation sites during this experiment justifies the development of iron thin films with amorphous structures.

3.3. Surface images of the amorphous iron films

Figure 6 shows SEM images of the amorphous iron films electrodeposited at an amplitude of

15.9 mAcm⁻², a deposition temperature of 276 K, and a duty cycle of 60 %.

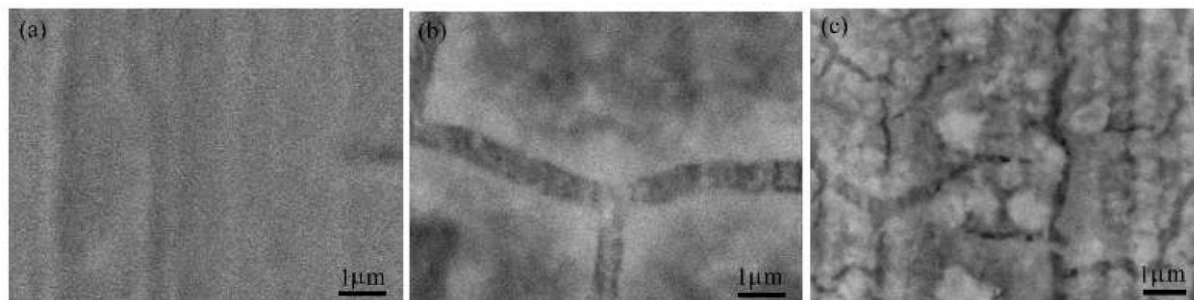


Figure 6. SEM images of the iron thin films electrodeposited at an amplitude of 15.9 mAcm⁻² and duty cycle of 50%. The iron thin films had thickness of (a) 0.03, (b) 0.12, and (c) 1.1 μm, respectively.

At the initial growth stage, the surface of the iron thin film appeared to be very smooth [18] as shown in Fig. 6 (a); however, as the growth proceeded, the amorphous films became increasingly cracked, but did not detach from the copper plate.

4. CONCLUSIONS

In this study, several iron films were electrodeposited using a rectangle pulse current (at a rate of 2 MHz); subsequently, the transition between polycrystalline and amorphous structures was analyzed in detail by XRD. The minimum mean grain size estimated by the Scherrer equation reached a minimum value under a rectangular pulse current with a specific amplitude and duty cycle. Overall, it was noticed that the minimum grain size decreased with the deposition temperature. In conclusion, the process described in this paper allowed the successful production of amorphous iron films at the deposition temperature ≤ 295 K and duty cycle ≥ 40 %.

References

1. X. Y. Yang, B. Yang, X. P. Li, Y. Cao, and R. H. Yu, *J. Alloy. Compd.*, 651 (2015) 551.
2. J. Shi, *Nanomedicine (Lond.)*, 11 (2016) 1189.
3. S. Gypser, F. Hirsch, A. M. Schleicher, and D. Freese, *J. Environ. Sci.*, 70 (2018) 175.
4. Z-D. Liu, H-C. Wang, Q. Zhou, and R-K. Xu, *Ecotox. Environ. Safe.*, 145 (2017) 207.
5. Z. Jia, J. Kang, W. C. Zhang, W. M. Wang, C. Yang, H. Sun, D. Habibi, and L. C. Zhang, *Appl. Catal. B: Environ.*, 204 (2017) 537.
6. L. M. Boichyshyn, Y. O. Kulyk, O. M. Hertsyk, B. Y. Kotur, O. Y. Rudenko, and M. S. Nizameev, *Mater. Sci.*, 52 (2017) 854
7. J-F. Huang, Y-T. Li, J-H. Wu, X-M. Dong, P-Y. Cao, Y-L. Liu, Z-T. Lin, and G-B. Jiang, *Compos. Sci. and Technol.*, 134 (2016) 168
8. R. Maizi, P. Fricoteaux, A. Mohamadou, A. Meddour, and C. Rousse, *Int. J. Electrochem. Sci.*, 11 (2016) 7111.
9. J. Ordoukhanian, H. Karami, and A. Nezhadal, *Mater. Sci.-Poland*, 34 (2016) 655.

10. D. V. Kumar, S. Ayyagari, and M. J. N. V. Prasad, *Mater. Chem. Phys.*, 201 (2017) 26.
11. G. Panzeri, A. Accogli, E. Gibertini, C. Rinaldi, L. Nobili, and L. Magagnin, *Electrochim. Acta*, 271 (2018) 576.
12. U. Reuter, *J. Electroanal. Chem.*, 136 (1992) 167.
13. R. K. Pandey, S. N. Sahu, and S. Chandra, *Handbook of Semiconductor Electrodeposition*, Marcel Dekker, Inc., (1996) New York, USA.
14. Y-R. Kim, S. C. S. Lai, G. Zhang, D. Perry, T. S. Miller, and P. R. Unwin, *J. Phys. Chem. C*, 119 (2015) 17389.
15. M. Avrami, *J. Chem. Phys.*, 7 (1939) 1103.
16. M. Avrami, *J. Chem. Phys.*, 8 (1940) 212.
17. W. K. Burton, N. Cabrera, and F. C. Frank, *Proc. R. Soc. Lond. A*, 243 (1951) 299.
18. M. Saitou, *Int. J. Electrochem. Sci.*, 12 (2017) 1885.
19. JCPDS-ICDD Card No. 06-0696.
20. J. -M. Zhang, F. Ma, and K. -W. Xu, *Surf. Interface Anal.*, 35 (2003) 662.
21. C. Herring, *Phys. Rev.*, 82 (1951) 87.
22. D. C. Cullity, *Elements of X-ray Diffraction*, Addison-Wesley, (1978) Massachusetts, USA.
23. D. Grujicic and B. Pesic, *Electrochim. Acta*, 50 (2005) 4405.
24. J. W. Evans, P. A. Thiel, and M. C. Bartelt, *Surf. Sci. Rep.*, 61 (2006) 1.
25. P. M. Chaikin and T. C. Lubensky, *Principles of Condensed Matter Physics*, Cambridge University Press, (2000) Cambridge, GB.

© 2020 The Authors. Published by ESG (www.electrochemsci.org). This article is an open access article distributed under the terms and conditions of the Creative Commons Attribution license (<http://creativecommons.org/licenses/by/4.0/>).